JOURNAL OF AIRCRAFT
Vol. 32, No. 6, November–December 1995

Rotor Free-Wake Modeling Using a Pseudoimplicit Relaxation Algorithm

Ashish Bagai* and J. Gordon Leishman†
University of Maryland, College Park, Maryland 20742

A pseudoimplicit predictor–corrector relaxation algorithm with five-point central differencing in space has been developed for the solution of the governing differential equations of the helicopter rotor free-wake problem. This new approach is compared and contrasted with more conventional explicit-type free-wake algorithms. A convergence analysis shows that the new algorithm provides for much more rapid convergence characteristics compared to explicit methods, with improvements in numerical efficiency and predictive accuracy.

Nomenclature

$\boldsymbol{bc}$	=	spatial boundary condition vector
C_T	=	rotor thrust coefficient, $T/\rho\pi R^2(\Omega R)^2$
c	=	blade chord, m
E	=	shift operator
$\hat{\imath}, \hat{\jmath}, \hat{k}$	=	unit vectors in the x, y, and z directions, respectively
L	=	spatial discretization operator
l	=	length of discretized vortex element, m
N_b	=	number of blades
N_w	=	number of vortex filaments
P	=	iteration scheme operator
R	=	rotor radius, m
r_c	=	vortex core radius, m
r_w	=	spanwise location from which vortex filaments are trailed, m
$\boldsymbol{r}$	=	position vector of a point on a vortex filament, m
$\boldsymbol{S}$	=	source vector
T	=	rotor thrust, N
t	=	time, s
V_∞	=	freestream velocity, m/s
$\boldsymbol{V}$	=	time invariant flowfield velocity, m/s
$\boldsymbol{V}_{\text{ind}}$	=	induced velocity, m/s
$\boldsymbol{V}_{\text{loc}}$	=	local velocity at a point in space, m/s
v_θ	=	tangential velocity, m/s
x, y, z	=	Cartesian coordinate system, origin at hub center
α_s	=	rotor shaft angle (negative forward), deg
β_0	=	blade coning angle, deg
Γ	=	circulation, m²/s
$\Delta\boldsymbol{r}^n$	=	nth iteration position–vector correction
ζ	=	distance along trailed wake filament (wake age), rad
λ_i	=	uniform-induced inflow ratio
μ	=	rotor advance ratio, $V_\infty/\Omega R$
ν	=	kinematic viscosity of air, m²/s
ψ	=	azimuth angle, rad
ψ_b	=	blade azimuth angle, rad
Ω	=	rotational frequency of rotor, rad/s

Introduction

THE improved modeling of a helicopter rotor flowfield remains fundamental to enhanced predictions of rotor loads, aircraft performance, and rotor acoustics. It has been documented experimentally that a helicopter rotor wake is dominated by strong tip vortices that quickly form and roll-up behind each blade.[1,2] The tip vortex strengths and positions relative to the rotor affect the induced velocity field and are known to be influenced by many interrelated geometric parameters (such as blade twist, planform, and number of blades) and operational conditions (such as rotor thrust, advance ratio, climb velocity, and tip path plane angle of attack). The presence of other rotors (such as a tail rotor or another main rotor), as well as rotor/airframe interference effects, further increase the overall physical complexity of the problem. Since the tip vortices are convected only relatively slowly away from the rotor, large spatial variations in induced velocity can be produced at each rotor blade. When coupled with velocity components due to rotor rotational and forward-flight translation, the resulting blade angle-of-attack variations give rise to highly three-dimensional, time-varying loads on each blade. The temporal variations in local blade loading may also result in impulsive noise generation from the rotor. Clearly, the ability to predict the performance and aeroacoustics of the entire vehicle is strongly dependent on the ability to accurately predict the highly interactive dynamics of the rotor wake.

The mathematical modeling of the helicopter rotor wake problem at any realistic level of sophistication is, unfortunately, a problem of formidable complexity. Modern comprehensive rotor codes typically include sophisticated structural and dynamic models of the rotor system, and there is a pressing need to invoke aerodynamic models with a comparable level of sophistication to ensure a fully coupled and physically realistic solution. Unfortunately, there are still several fundamental as well as practical issues that preclude the use of elaborate aerodynamic models of the rotor blades and its wake system. While considerable effort has already been invested in understanding and modeling the rotor wake problem, computationally efficient and properly validated rotor wake models do not yet exist. Furthermore, many models in current use exhibit numerical problems that seriously limit their application to many conditions of practical significance.

Rotor wake models range from fairly routine "prescribed" or semiempirical models, to more sophisticated "free" wake

Presented as Paper 94-1918 at the AIAA 12th Applied Aerodynamics Conference, Colorado Springs, CO, June 20–23, 1994; received July 14, 1994; revision received March 21, 1995; accepted for publication May 15, 1995.

*Graduate Research Assistant, Center for Rotorcraft Education and Research, A. James Clark School of Engineering, Glenn L. Martin Institute of Technology, Department of Aerospace Engineering.

†Associate Professor, Center for Rotorcraft Education and Research, A. James Clark School of Engineering, Glenn L. Martin Institute of Technology, Department of Aerospace Engineering. Senior Member AIAA.

models. References 3–6 describe typical prescribed wake models, where the rotor tip vortex trajectories are described by functional modifications to the classical or "rigid" cycloidal wake. Distortion functions are specified in terms of rotor geometric and operational factors with the aid of wake geometry measurements from small-scale isolated rotors.[7,8] The induced velocity field from the rotor wake is then calculated by the application of the Biot–Savart law integrated along the prescribed trajectory of each tip vortex filament. Although computationally efficient and of considerable use in routine rotor design work, prescribed wake models do not fully capture the physical nature of the wake. Furthermore, since these models are constructed based on a limited number of small-scale rotor experiments, their applicability to more general rotors or complete helicopter configurations is questionable. On the other hand, free-wake models solve for the rotor wake geometry directly, and in principle, do not require experimentally obtained wake geometry data for formulation purposes. However, since the positions of the individual wake filaments now become part of the solution process, free-wake models are obviously much more computationally intensive. Pioneering work on the free-wake solution methodology was performed about 20 years ago using an iterative scheme by Clark and Leiper[9] and a time-marching scheme by Landgrebe,[10] and many variations and developments of the basic approach have subsequently followed.[11–16]

In essence, the numerical solution to the free-wake problem can be described by the integration of a system of ordinary differential equations (ODEs) that are obtained by the spatial discretization of the partial differential equations (PDEs) that govern the wake problem. A series of collocation points are specified on the trailed vortex filaments generated by each blade and these points are continuously convected through the flowfield at the local velocity. The local velocity at each collocation point is calculated by the application of the Biot–Savart law to every vortex collocation point. The solution then proceeds either in a time-marching sense or iteratively in a relaxation scheme. While free-wake models may be considered to more faithfully represent the physics of the rotor flowfield than prescribed wakes, their practical usefulness has been beset by large computational requirements as well as various numerical issues. These numerical problems include susceptibility to instabilities and sensitivity to time (azimuth) discretization. These are particular problems for hover and low-speed forward flight, where the close mutual interaction of the tip vortex filaments results in high local induced velocities, and often large nonphysical perturbations to the wake can be produced. Several studies have focused on this problem, and have found that some wake instabilities in time-marching free-wake schemes can be avoided by using numerical damping, such as artificially large-tip vortex core radii and/or an averaging/smoothing scheme.[11,12] This implies that the lack of convergence exhibited by some free-wake methods is more numerical rather than physical. However, physical instabilities on helical vortex filaments such as those found from rotors are also known to exist.[17]

In this article, we examine a new approach to the prediction of the wake geometry generated by helicopter rotors operating in hover or forward (edgewise) flight. The approach uses five-point spatial discretization of the governing equations and the wake is allowed to relax iteratively using a pseudoimplicit predictor–corrector method. The explicit-type free-wake modules used in many modern rotor analyses[18,19] are known to exhibit several numerical problems such as instabilities and/or poor convergence. The need to fully resolve these issues has partly motivated the current work. Also, there was a need to formulate models that were physically more accurate and numerically more robust to handle problems in multirotor aerodynamics, acoustics, and rotor/airframe interaction studies. The emphasis in this article is mostly on numerical details of the new algorithm.

Methodology

Background

Depending upon the solution approach, free-wake models can be divided into two general types of methodologies: 1) time-stepping and 2) relaxation schemes. Furthermore, different integration schemes can be used within each approach, i.e., explicit, implicit, or hybrid schemes. In the most basic free-wake methodology, an explicit algorithm is used to extrapolate the wake geometry to the next time step in the time domain. Explicit-type algorithms are used in several well-known comprehensive rotor codes; however, one of the well-known problems of explicit schemes is their susceptibility to numerical instabilities.[20] Small time steps can be used to minimize this problem, but most rotor codes require the discretization of the wake into fairly large segments (usually 15–30-deg blade azimuth segments per rotor revolution) to keep the computational effort for the aerodynamics within practical limits. At such coarse levels of discretization, the fidelity of the velocity field calculation can be compromised, and the corresponding wake dynamics can be accompanied by large truncation errors and poor overall convergence characteristics.

One solution to these numerical problems is to implement improved integration schemes. Several such implementations are possible, but usually at the expense of significantly increasing the overall computational expense, often making many approaches impractical for routine use in comprehensive rotor analyses. Miller and Bliss[16] showed that by bypassing the time domain and enforcing periodicity in the azimuthal direction, as well as by using a semi-implicit formulation for the wake solution, many of the numerical problems that are characteristic of explicit free-wake models could be avoided. However, implicit schemes require the inversion of large matrices per iteration/time step, making them computationally very expensive for use in comprehensive rotor codes.

More recently, Crouse and Leishman[21] showed that a hybrid predictor–corrector free-wake method with spatial averaging can be used to stabilize the numerical computation. Because of improved convergence relative to single-step schemes, the overall computational expense can be reduced. Such an approach draws a good compromise between minimizing numerical errors and helping to maximize computational efficiency. While fairly good convergence characteristics were obtained in hover and low-speed forward flight, some artificial damping between successive velocity field updates was required, even at higher speed forward-flight conditions.

Free-Wake Equations

Physically, it is known that each rotor blade trails a concentrated vortex from the vicinity of the blade tip. The formation of the tip vortex is known to be a physically complex process involving flow separation, yet it is known that rotors develop single concentrated vortices almost immediately behind the blade tip (at least with blades that have conventional tip shapes). The strength and radial location of this vortex at any given azimuth position is determined by the magnitude of the blade life and spanwise lift distribution.

In the present analysis, the rotor wake system is decomposed into two main parts. The first is a near-wake model of trailed and shed vorticity behind each blade. The second is a far wake comprising the rolled-up tip vortices from the blades. The numerical treatment of the near wake is a separate but related problem, and can be based on several models ranging from a simple lifting line to more advanced computational fluid dynamics (CFD) models. The near-wake model defines the initial strengths and locations of the rolled-up blade-tip vortices and defines a boundary condition for the free-wake problem. In the present work, the initial tip vortex strength and release position was computed based on Rossow's cen-

troid of vorticity approach.[22] This then forms a boundary condition to the free-wake problem. Thereafter, it is assumed that the individual vortex filaments in the flowfield are convected to force-free positions at the local flow velocity.

As described in Ref. 23, the PDE governing the geometry of a free-tip vortex in the rotor wake can be written as

$$\frac{\partial \boldsymbol{r}(\psi, \zeta)}{\partial \psi} + \frac{\partial \boldsymbol{r}(\psi, \zeta)}{\partial \zeta} = \frac{1}{\Omega}\left\{\boldsymbol{V}_\infty + \sum_{i=1}^{N_v} \boldsymbol{V}_{\text{ind}}[\boldsymbol{r}(\psi, \zeta), \boldsymbol{r}(\psi_i, \zeta)]\right\} \tag{1}$$

where the V_{ind} term on the right-hand side (RHS) collectively represents the velocities induced by the lifting blades and all the free vortices in the wake. In addition, there may be other contributions to the velocity field from the airframe or another rotor, such as a tail rotor. In the present article, we will concentrate on the free vortices in the rotor wake, as generated by a single main rotor. The induced velocity from the free vortices can be computed by using the well-known Biot–Savart law where

$$\boldsymbol{V}_{\text{ind}}[\boldsymbol{r}(\psi, \zeta), \boldsymbol{r}(\psi_i, \zeta)] \equiv \frac{1}{4\pi}\int \frac{\Gamma(\psi_i, \zeta)\, d\boldsymbol{\zeta}_i \times [\boldsymbol{r}(\psi, \zeta) - \boldsymbol{r}(\psi_i, \zeta)]}{|\boldsymbol{r}(\psi, \zeta) - \boldsymbol{r}(\psi_i, \zeta)|^3} \tag{2}$$

and where $\boldsymbol{r}(\psi, \zeta)$ is the point in the flowfield influenced by the ith vortex at location $\boldsymbol{r}(\psi_i, \zeta)$ and of strength (circulation) $\Gamma(\psi_i, \zeta)$. These induced velocities produce the highly nonlinear space and time-dependent forcing functions or source terms that describe the physical nature of the problem.

Discretization of Wake Equations

Any numerical scheme used to integrate the governing equations of the wake requires that the physical domain be discretized into a finite computational domain. Care must be taken during the discretization process, however, to retain the physical structure of the problem. The tip vortices in the free-wake are subdivided into smaller straight-line segments. Note that in a discretized sense there is one equation such as Eq. (1) for every point in the wake. Clearly, the number of segments determines the wake resolution, but also increases the magnitude of the numerical problem. The discretized physical domain for one rotor blade is shown in Fig. 1. For

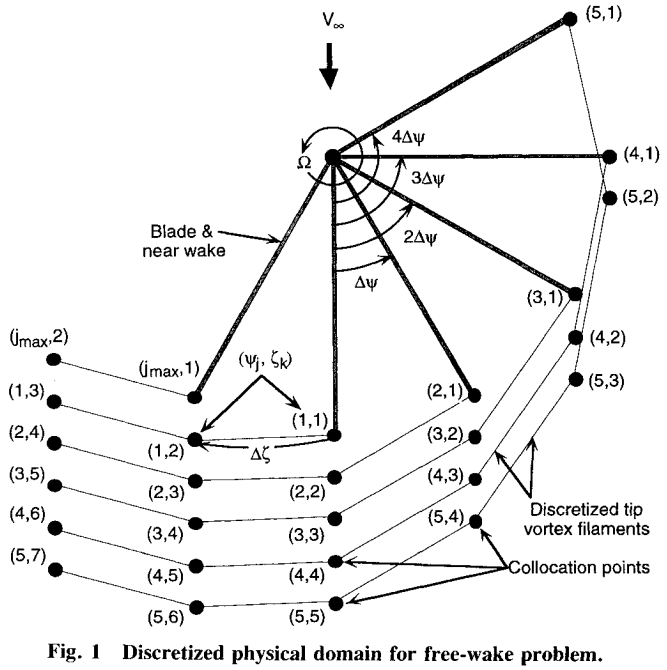

Fig. 1 Discretized physical domain for free-wake problem.

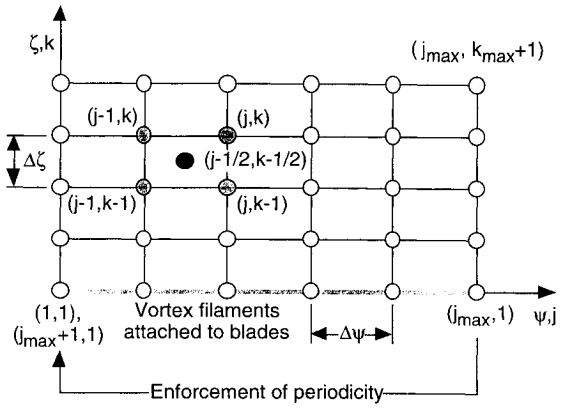

Fig. 2 Discretized computational domain for free-wake problem.

the solution of the wake equations, Eq. (1) must first be transformed into a finite difference equation. In the present work, a five-point central difference approximation is used, where the partial derivatives on the left-hand side are evaluated at the central point $(j - \frac{1}{2}, k - \frac{1}{2})$ about points (j, k), $(j, k - 1)$, $(j - 1, k)$, and $(j - 1, k - 1)$. The velocity or source terms on the RHS are also evaluated at the central point using an average of the velocity at its four neighboring points. The computational domain for this finite difference scheme is shown in Fig. 2.

A relaxation approach that bypasses the time domain has been adopted in the present work. This introduces an iteration index, denoted by n, into the discretized PDEs. A single-step, fully explicit FDE can be written in the following point operator form:

$$\begin{aligned}\boldsymbol{r}^n_{j,k} = {} & \boldsymbol{r}^{n-1}_{j-1,k-1} + \left(\frac{\Delta\psi - \Delta\zeta}{\Delta\psi + \Delta\zeta}\right)(\boldsymbol{r}^{n-1}_{j,k-1} - \boldsymbol{r}^{n-1}_{j-1,k}) \\ & + \left(\frac{\Delta\psi\Delta\zeta}{\Delta\psi + \Delta\zeta}\right)\frac{2}{\Omega}\left\{\boldsymbol{V}_\infty + \frac{1}{4}\left[\sum_{i=1}^{N_v} \boldsymbol{V}_{\text{ind}}(\boldsymbol{r}^{n-1}_{j-1,k-1}, \boldsymbol{r}^{n-1}_{i,\zeta}) \right.\right. \\ & + \sum_{i=1}^{N_v} \boldsymbol{V}_{\text{ind}}(\boldsymbol{r}^{n-1}_{j-1,k}, \boldsymbol{r}^{n-1}_{i,\zeta}) + \sum_{i=1}^{N_v} \boldsymbol{V}_{\text{ind}}(\boldsymbol{r}^{n-1}_{j,k-1}, \boldsymbol{r}^{n-1}_{i,\zeta}) \\ & \left.\left. + \sum_{i=1}^{N_v} \boldsymbol{V}_{\text{ind}}(\boldsymbol{r}^{n-1}_{j,k}, \boldsymbol{r}^{n-1}_{i,\zeta})\right]\right\}\end{aligned} \tag{3}$$

Note that in the previous scheme, the solution at the current iteration is obtained by extrapolating the solution from the previous iteration over a finite "time" increment $\Delta\psi$ by means of a single backward finite difference step, i.e., $\boldsymbol{r}^n_{j,k} = f(\boldsymbol{r}^{n-1}_{j-1,k-1}, \boldsymbol{r}^{n-1}_{j-1,k}, \boldsymbol{r}^{n-1}_{j,k-1})$ and $\boldsymbol{V}_{\text{ind}} = g(\boldsymbol{r}^{n-1}_{j-1,k-1}, \boldsymbol{r}^{n-1}_{j-1,k}, \boldsymbol{r}^{n-1}_{j,k-1})$. Although this may be one of the simplest methods to implement, it is only first-order accurate and the accumulation of discretization errors over a number of iterations often result in the method becoming numerically unstable. Therefore, such methods often require the inclusion of some form of numerical damping to prevent instabilities from developing.

Various improvements in the accuracy and stability of explicit schemes may be made by using a predictor–corrector methodology, and often without the need for numerical damping. In this approach, the predicted solution at the nth iteration using an explicit step [such as Eq. (3)] is corrected by averaging the induced velocity from the previous $(n - 1)$th iteration with the predicted induced velocities from the current nth iteration predictor step. The enhanced stability and increased convergence rates of such schemes normally outweigh the additional computational expense of performing two induced velocity calculations per iteration compared to

the single-step explicit method. In point operator notation, the corrector equation can be written as

$$\begin{aligned} \boldsymbol{r}^n_{j,k} &= \boldsymbol{r}^{n-1}_{j-1,k-1} + \left(\frac{\Delta\psi - \Delta\zeta}{\Delta\psi + \Delta\zeta}\right)(\boldsymbol{r}^{n-1}_{j,k-1} - \boldsymbol{r}^{n-1}_{j-1,k}) \\ &+ \left(\frac{\Delta\psi\Delta\zeta}{\Delta\psi + \Delta\zeta}\right)\frac{2}{\Omega}\left\{\boldsymbol{V}_\infty + \frac{1}{4}\left[\sum_{i=1}^{N_v}\tilde{\boldsymbol{V}}_{\text{ind}}(\boldsymbol{r}_{j-1,k-1}, \boldsymbol{r}_{i,\zeta})\right.\right. \\ &+ \sum_{i=1}^{N_v}\tilde{\boldsymbol{V}}_{\text{ind}}(\boldsymbol{r}_{j-1,k}, \boldsymbol{r}_{i,\zeta}) + \sum_{i=1}^{N_v}\tilde{\boldsymbol{V}}_{\text{ind}}(\boldsymbol{r}_{j,k-1}, \boldsymbol{r}_{i,\zeta}) \\ &\left.\left. + \sum_{i=1}^{N_v}\tilde{\boldsymbol{V}}_{\text{ind}}(\boldsymbol{r}_{j,k}, \boldsymbol{r}_{i,\zeta})\right]\right\} \end{aligned} \tag{4}$$

where the velocity terms on the RHS of the previous equation are given by

$$\begin{aligned} &\tilde{\boldsymbol{V}}_{\text{ind}}(\boldsymbol{r}_{j-1,k-1}, \boldsymbol{r}_{i,\zeta}) \\ &\quad = \tfrac{1}{2}[\boldsymbol{V}_{\text{ind}}(\boldsymbol{r}^{n-1}_{j-1,k-1}, \boldsymbol{r}^{n-1}_{i,\zeta}) + \boldsymbol{V}_{\text{ind}}(\tilde{\boldsymbol{r}}^{n}_{j-1,k-1}, \tilde{\boldsymbol{r}}^{n}_{i,\zeta})] \\ &\tilde{\boldsymbol{V}}_{\text{ind}}(\boldsymbol{r}_{j-1,k}, \boldsymbol{r}_{i,\zeta}) = \tfrac{1}{2}[\boldsymbol{V}_{\text{ind}}(\boldsymbol{r}^{n-1}_{j-1,k}, \boldsymbol{r}^{n-1}_{i,\zeta}) + \boldsymbol{V}_{\text{ind}}(\tilde{\boldsymbol{r}}^{n}_{j-1,k}, \tilde{\boldsymbol{r}}^{n}_{i,\zeta})] \\ &\tilde{\boldsymbol{V}}_{\text{ind}}(\boldsymbol{r}_{j,k-1}, \boldsymbol{r}_{i,\zeta}) = \tfrac{1}{2}[\boldsymbol{V}_{\text{ind}}(\boldsymbol{r}^{n-1}_{j,k-1}, \boldsymbol{r}^{n-1}_{i,\zeta}) + \boldsymbol{V}_{\text{ind}}(\tilde{\boldsymbol{r}}^{n}_{j,k-1}, \tilde{\boldsymbol{r}}^{n}_{i,\zeta})] \\ &\tilde{\boldsymbol{V}}_{\text{ind}}(\boldsymbol{r}_{j,k}, \boldsymbol{r}_{i,\zeta}) = \tfrac{1}{2}[\boldsymbol{V}_{\text{ind}}(\boldsymbol{r}^{n-1}_{j,k}, \boldsymbol{r}^{n-1}_{i,\zeta}) + \boldsymbol{V}_{\text{ind}}(\tilde{\boldsymbol{r}}^{n}_{j,k}, \tilde{\boldsymbol{r}}^{n}_{i,\zeta})] \end{aligned} \tag{5}$$

The position vectors $\tilde{\boldsymbol{r}}^n_{\cdots,\cdots}$ are predicted values returned by the explicit predictor step given by Eq. (3).

A further improvement in the predictor–corrector scheme can be made by realizing that the collocation point position vectors on the RHS of Eqs. (3) and (4) are for locations $(j-1, k-1)$, $(j, k-1)$, and $(j-1, k)$. Since all these points have already been calculated at the current iteration, the vectors $\boldsymbol{r}^{n-1}_{j-1,k-1}$, $\boldsymbol{r}^{n-1}_{j,k-1}$, and $\boldsymbol{r}^{n-1}_{j-1,k}$ on the RHS of Eqs. (3) and (4) can be replaced by vectors $\boldsymbol{r}^{n}_{j-1,k-1}$, $\boldsymbol{r}^{n}_{j,k-1}$, and $\boldsymbol{r}^{n}_{j-1,k}$, respectively. This results in a pseudoimplicit scheme for both the predictor and corrector steps, which can be written as follows:

Predictor

$$\begin{aligned} \tilde{\boldsymbol{r}}^n_{j,k} &= \tilde{\boldsymbol{r}}^n_{j-1,k-1} + \left(\frac{\Delta\psi - \Delta\zeta}{\Delta\psi + \Delta\zeta}\right)(\tilde{\boldsymbol{r}}^n_{j,k-1} - \tilde{\boldsymbol{r}}^n_{j-1,k}) \\ &+ \left(\frac{\Delta\psi\Delta\zeta}{\Delta\psi + \Delta\zeta}\right)\frac{2}{\Omega}\left\{\boldsymbol{V}_\infty + \frac{1}{4}\left[\sum_{i=1}^{N_v}\boldsymbol{V}_{\text{ind}}(\boldsymbol{r}^{n-1}_{j-1,k-1}, \boldsymbol{r}^{n-1}_{i,\zeta})\right.\right. \\ &+ \sum_{i=1}^{N_v}\boldsymbol{V}_{\text{ind}}(\boldsymbol{r}^{n-1}_{j-1,k}, \boldsymbol{r}^{n-1}_{i,\zeta}) + \sum_{i=1}^{N_v}\boldsymbol{V}_{\text{ind}}(\boldsymbol{r}^{n-1}_{j,k-1}, \boldsymbol{r}^{n-1}_{i,\zeta}) \\ &\left.\left. + \sum_{i=1}^{N_v}\boldsymbol{V}_{\text{ind}}(\boldsymbol{r}^{n}_{j,k}, \boldsymbol{r}^{n-1}_{i,\zeta})\right]\right\} \end{aligned} \tag{6}$$

Corrector

$$\begin{aligned} \boldsymbol{r}^n_{j,k} &= \boldsymbol{r}^n_{j-1,k-1} + \left(\frac{\Delta\psi - \Delta\zeta}{\Delta\psi + \Delta\zeta}\right)(\boldsymbol{r}^n_{j,k-1} - \boldsymbol{r}^n_{j-1,k}) \\ &+ \left(\frac{\Delta\psi\Delta\zeta}{\Delta\psi + \Delta\zeta}\right)\frac{2}{\Omega}\left\{\boldsymbol{V}_\infty + \frac{1}{4}\left[\sum_{i=1}^{N_v}\tilde{\boldsymbol{V}}_{\text{ind}}(\boldsymbol{r}_{j-1,k-1}, \boldsymbol{r}_{i,\zeta})\right.\right. \\ &+ \sum_{i=1}^{N_v}\tilde{\boldsymbol{V}}_{\text{ind}}(\boldsymbol{r}_{j-1,k}, \boldsymbol{r}_{i,\zeta}) + \sum_{i=1}^{N_v}\tilde{\boldsymbol{V}}_{\text{ind}}(\boldsymbol{r}_{j,k-1}, \boldsymbol{r}_{i,\zeta}) \\ &\left.\left. + \sum_{i=1}^{N_v}\tilde{\boldsymbol{V}}_{\text{ind}}(\boldsymbol{r}_{j,k}, \boldsymbol{r}_{i,\zeta})\right]\right\} \end{aligned} \tag{7}$$

where the induced velocity vectors $\tilde{\boldsymbol{V}}_{\text{ind}}(\cdots, \cdots)$, are defined in Eq. (5). Note, however, that the source terms [which are comprised of the induced velocities on the RHS of Eq. (7)] are still treated explicitly, in that the final values for the induced velocities are computed using averages of the previous iteration values and the predicted values from the current iteration.

Such predictor–corrector methods have a truncation error per step of order $\Delta\psi^3$ and better stability characteristics than single-step methods alone. Also, they require considerably less computation than implicit or semi-implicit schemes. Recall, however, that the predictor–corrector scheme requires two velocity field calculations per time step compared to the explicit method.

Boundary Conditions

Since the PDE governing the free-wake problem is first order in ψ and ζ, the solution of the problem requires the specification of one initial/boundary condition in the ψ direction, and one boundary condition in the ζ direction. Note that while ζ is a spatial coordinate, ψ can be interpreted as either a temporal coordinate (as would be the case for time-stepping schemes), or as a spatial coordinate (as in the present case) when incorporating a relaxation methodology.

The relaxation method specifies that the trailed vortex elements be attached to the blades (or, more strictly, the near wake) as an "initial-boundary" condition in the ζ direction for each ψ, whereas wake periodicity is enforced as the boundary condition in the ψ direction (see Fig. 2). The solution is stepped in the ζ direction in an iterative manner and convergence is obtained once the wake geometry no longer distorts between successive iterations. Mathematically, the boundary and initial conditions may be stated as follows:

Boundary conditions

$$\boldsymbol{r}(\psi, \zeta) = \boldsymbol{r}(\psi + 2\pi, \zeta) \tag{8}$$

Initial-boundary conditions ($\zeta = 0$)

$$\begin{aligned} \boldsymbol{r}(\psi, 0) &= r_v[\cos(\beta_0)\cos(\psi)\cos(\alpha_s) + \sin(\beta_0)\sin(\alpha_s)]\hat{\imath} \\ &+ r_v[\cos(\beta_0)\sin(\psi)]\hat{\jmath} + r_v[\sin(\beta_0)\cos(\alpha_s) \\ &- \cos(\beta_0)\cos(\psi)\sin(\alpha_s)]\hat{\boldsymbol{k}} \end{aligned} \tag{9}$$

In addition to the boundary and initial conditions, an initial prescribed wake geometry is used to start the free-wake calculations. In its simplest form, this can be an undistorted wake as given by

$$\begin{aligned} \boldsymbol{r}(\psi, \zeta) &= (r_v[\cos(\beta_0)\cos(\psi - \zeta)\cos(\alpha_s) + \sin(\beta_0)\sin(\alpha_s)] \\ &- R\{\lambda_i[-\cos(\alpha_s)\cos(\psi - \zeta)\sin(\beta_0) + \sin(\alpha_s)\cos(\beta_0)] \\ &+ \mu\zeta\})\hat{\imath} + \{r_v[-\cos(\beta_0)\sin(\psi - \zeta)] \\ &+ R\lambda_i \sin(\psi - \zeta)\sin(\beta_0)\}\hat{\jmath} + (r_v[\sin(\beta_0)\cos(\alpha_s) \\ &- \cos(\beta_0)\cos(\psi - \zeta)\sin(\alpha_s)] \\ &- R\{\lambda_i[\sin(\alpha_s)\cos(\psi - \zeta)\sin(\beta_0) \\ &+ \cos(\alpha_s)\cos(\beta_0)]\zeta\})\hat{\boldsymbol{k}} \end{aligned} \tag{10}$$

For relaxation methods, the initial prescribed wake is used only to set up an approximate initial induced velocity field. In practice, it has been found that because wake convergence is so rapid with the present scheme the convergence rate and final solution is insensitive to these initial conditions.

Convergence Criterion

It is necessary to impose a convergence criterion on the relaxation scheme. In the present work, this has been based on a measure of the L_2 norm of the change in the tip vortex

geometry locations between two successive wake iterations. Convergence is reached after the L_2 norm (rms) drops below a certain prescribed threshold between two successive wake iterations. In practice, this change must fall to an order of $\sim 10^{-4}$ to ensure that the wake has fully converged. It is known through numerical experimentation that the wake exhibits no appreciable change in wake geometry once this condition has been satisfied.

Vortex Model

The crux of determining the induced effects of the wake on the rotor blades, as well as the mutually induced interactions between vortex filaments in the rotor wake, depends on the vortex model and evaluation of the Biot–Savart integral. The source terms on the RHS of Eq. (1) are comprised of the steady freestream velocity component and the total induced influence of all the vortices in the wake. If a potential model is assumed for the free vortices, then the induced velocity due to a vortex element becomes singular when the point of evaluation approaches the vortex axis. Obviously, this will result in a nonphysical solution for the wake geometry and may also result in numerical problems. This can be alleviated by using a viscous vortex model with a finite core radius. The source terms of Eq. (1) can be rewritten as

$$\boldsymbol{V}[\boldsymbol{r}(\psi, \zeta)] = \boldsymbol{V}_\infty + \frac{h^2}{4\pi\sqrt{r_c^4 + h^4}} \times \sum_{j=1}^{N_v} \int \frac{\Gamma(\psi_j, \zeta)\, d\boldsymbol{\zeta}_j \times [\boldsymbol{r}(\psi, \zeta) - \boldsymbol{r}(\psi_j, \zeta)]}{|\boldsymbol{r}(\psi, \zeta) - \boldsymbol{r}(\psi_j, \zeta)|^3} \tag{11}$$

where r_c is the instantaneous vortex core radius and h is the perpendicular distance of the evaluation point $\boldsymbol{r}(\psi, \zeta)$ from the jth influencing vortex element located at $\boldsymbol{r}(\psi_j, \zeta)$ and of orientation $d\boldsymbol{\zeta}_j$.

In the present analysis, the vortex core radius is allowed to vary as a function of wake age (or time) in a manner consistent with the decay of a laminar Lamb–Oseen vortex,[24,25] and can be represented using

$$r_c(\zeta) = 2.24\sqrt{\nu\delta(\zeta/\Omega)} \tag{12}$$

The factor δ is an "eddy" or turbulent viscosity coefficient, which must be selected empirically. For a laminar vortex, δ has a value of unity, yet with this value the diffusion of the tip vortex is unrealistically slow. Various researchers have shown that it is possible to allow for an eddy viscosity, which is essentially due to the degree of turbulence in the flow, and adjusting the value of δ by comparisons of calculation with experiment.[24–26] Note according to Eq. (12) the ideal tip vortex starts with a zero-core radius, which grows parabolically with age, and therefore, no assumptions need be made with regard to a starting core radius. In practice, however, the physical rollup of a rotor tip vortex is quite complicated, involving flow separation, and produces a vortex that is already in some stage of decay. Equation (12) can accordingly be modified to represent a variety of initial core radii and growth rates.

In addition to the physics of diffusion, the possibility of vorticity intensification due to straining of the vortex filaments must be considered. In some locations, particularly in regions where the tip vortex filaments rollup into bundles, considerable straining is possible. While an exact treatment of this problem is obviously impractical within the scope of the present model, a representation of the basic effect can be made using a simpler approach. If the vorticity is assumed to lie entirely within the core r_c, then the application of conservation of mass and angular momentum leads to the following relationship between the filament strain and the change in the local core size:

$$\Delta r_c = r_c\{\sqrt{[l/(1 + \Delta l)]} - 1\} \tag{13}$$

In practice, however, it has been found that this effect tends to have a small influence on the overall structure of the wake, which is dominated more by viscous diffusion.

Results and Discussion

Convergence Analysis

The free-wake problem is governed by the highly nonlinear, unsteady source terms comprising the self- and mutually induced velocities due to the free-tip vortices in the flow. These induced velocities cause the tip vortices to interact with each other and convect to force-free equilibrium positions in the rotor wake. Furthermore, these self- and mutual-interactions also result in the trailed vortices acquiring a highly distorted structure relative to the skewed helical wake given by Eq. (10). The following discussion deals with the numerical behavior of two explicit relaxation solution methodologies as previously introduced in Eq. (3) and Eqs. (6) and (7).

It is advantageous to first introduce the standard delta form of representing finite difference equations. In terms of spatial and temporal discretizations, the generalized delta form of a finite difference equation can be written as

$$P\Delta\boldsymbol{r}_{j,k}^n + L\boldsymbol{r}_{j,k}^n = \boldsymbol{S} \tag{14}$$

where $\Delta\boldsymbol{r}_{j,k}^n = \boldsymbol{r}_{j,k}^{n+1} - \boldsymbol{r}_{j,k}^n$ is the nth iteration correction, and the operator P represents the iteration (relaxation) method and is, therefore, scheme dependent. The L operator, on the other hand, represents the spatial discretization of the problem and is common to both the schemes being considered. The RHS vector $\boldsymbol{S}$ represents the source terms, which for the present problem is comprised of the steady freestream velocity as well as the unsteady, nonlinear self-, and mutually induced velocities due to the tip vortices in the wake. Other physical effects such as the distortion to the flowfield made by an airframe may also be included into the source terms, if required.

The L operator for the present spatial discretization can be written in terms of shift operators E (see Appendix A) in the following forms:

Nonuniform mesh

$$L = (1/2\Delta\psi)(1 - E_\psi^{-1} + E_\zeta^{-1} - E_\psi^{-1}E_\zeta^{-1}) + (1/2\Delta\zeta)(1 + E_\psi^{-1} - E_\zeta^{-1} - E_\psi^{-1}E_\zeta^{-1}) \tag{15}$$

Uniform mesh

$$L = (1/\Delta\psi)(1 - E_\psi^{-1}E_\zeta^{-1}) \tag{16}$$

whereas the P operator for the two methods can be written as follows.

Fully Explicit Scheme [Eq. (3)]

Nonuniform mesh

$$P = (1/2\Delta\psi) + (1/2\Delta\zeta) \tag{17}$$

Uniform mesh

$$P = 1/\Delta\psi \tag{18}$$

Pseudoimplicit Scheme [Eq. (6) or (7)]

Nonuniform mesh

$$P = (1/2\Delta\psi)(1 - E_\psi^{-1} + E_\zeta^{-1} - E_\psi^{-1}E_\zeta^{-1}) + (1/2\Delta\zeta)(1 + E_\psi^{-1} - E_\zeta^{-1} - E_\psi^{-1}E_\zeta^{-1}) \tag{19}$$

Uniform mesh

$$P = (1/\Delta\psi)(1 - E_{\psi}^{-1}E_{\zeta}^{-1}) \tag{20}$$

Using the previous P and L operators, the standard delta form can be rewritten in matrix notation as

$$\{\Delta \boldsymbol{r}^n\} = [P]^{-1}[-[L]\{\boldsymbol{r}^n\} - \{\boldsymbol{bc}\} + \{S\}] \tag{21}$$

Note that while the P and L operators are dissimilar for the explicit method [Eq. (3)], for the pseudoimplicit method [Eq. (6) or (7)], both of the operators are identical. For the two schemes, therefore, Eq. (21) can be simplified into the following:

Explicit

$$\{\Delta \boldsymbol{r}^n\} = -[P^{-1}L]\{\boldsymbol{r}^n\} - [P]^{-1}\{\boldsymbol{bc} - S\} \tag{22}$$

Pseudoimplicit

$$\{\Delta \boldsymbol{r}^n\} = -[I]\{\boldsymbol{r}^n\} - [P]^{-1}\{\boldsymbol{bc} - S\} \tag{23}$$

where $[I]$ is the identity matrix and $\boldsymbol{bc}$ is the (time invariant) boundary condition vector in the ζ direction.

Note that in the absence of induced velocity contributions from the rotor-tip vortices, (i.e., space and time-invariant source terms S = constant), Eq. (23) shows that the pseudoimplicit method will converge to the exact solution (undistorted, skewed helix, or epicycloidal wake) as given by Eq. (10) in one iteration (see Appendix B). Equation (10) is the exact analytical solution of Eq. (1) with boundary and initial conditions given by Eqs. (8) and (9), respectively, with the source terms on the RHS of Eq. (1) replaced by a uniform or time invariant velocity vector composed of only longitudinal and vertical velocity components, i.e.,

$$\boldsymbol{V} = V_{\infty}\hat{\boldsymbol{\imath}} + \Omega R\lambda_i\hat{\boldsymbol{k}} \tag{24}$$

With the source terms set to zero, the pseudoimplicit predictor–corrector scheme gives an rms difference of less than 10^{-7} between the initial wake and that obtained after one iteration. On the other hand, the single-step explicit method converges to the same analytical solution, but only after numerous iterations, since $[P^{-1}L] \neq [I]$. In fact, with the explicit scheme, as many iterations as wake collocation points are usually required for a converged solution because information is propagated through the computational domain only one point at a time. Of course, this undistorted wake geometry is physically unrealistic since in reality the mutual interactions between the rotor tip vortices are by no means negligible. Nevertheless, the geometry represented by Eq. (10) lays the foundation for simpler "prescribed wake models" that use semiempirical distortion functions to create a more realistic wake geometry and account for these mutual interactional effects.

The evolution of the wake will now be shown using both methods, but with active source terms. In general, the single-step explicit method exhibits very slow convergence characteristics. It is also interesting to note the periodicity of the oscillations in the convergence trend of the single-step explicit method. Since information is propagated to the next wake collocation point only after the upstream regions have locally converged, the wake experiences a perturbation every nine iterations. (Note, for a four-bladed rotor, the angle between the blades is 90 deg. For a discretization resolution of 10 deg this results in a blade passage perturbation every 90/10 deg or nine iterations.) Although this explicit scheme will ultimately converge to a unique solution, it obviously will take many iterations. On the other hand, for the pseudoimplicit, two-step predictor–corrector scheme, the "implicitness" of the position vectors on the RHS of the equations results in

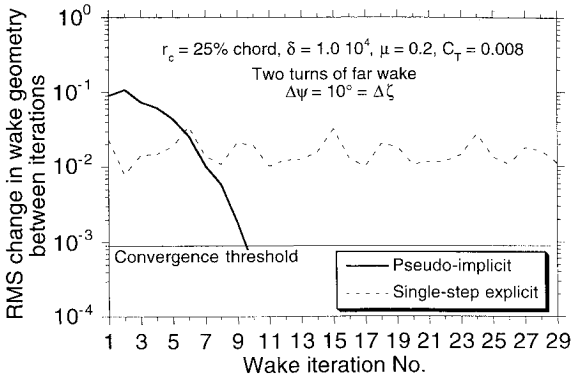

Fig. 3 Convergence histories for the pseudoimplicit and single-step explicit methods.

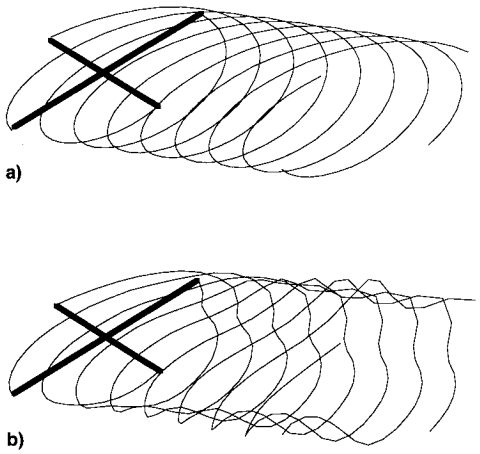

Fig. 4 Isometric views of converged wake geometries, $\mu = 0.23$, $\Delta\psi = \Delta\zeta = 10$ deg and two turns of far wake: a) inactive and b) active source terms.

information being propagated throughout the flowfield at every iteration. These trends are also reflected in the convergence histories of the two methods shown in Fig. 3, which are for equal temporal/spatial step sizes. Note, however, that since a two-step predictor–corrector scheme involves two induced velocity calculations per iteration as compared to a single-step method, the computational expense of n iterations of the two-step predictor–corrector method is roughly equivalent to the computational cost of $n/2$ iterations of the simple single-step method. While the use of some form of numerical damping for the geometry update can be used to help alleviate the oscillations in convergence, this results in even slower convergence trends. The pseudoimplicit predictor–corrector scheme on the other hand, shows monotonic convergence since every point in the computational domain is updated at each iteration.

A comparison between the undistorted wake geometry with the converged wake geometry obtained with source terms active is shown in an isometric view in Fig. 4. Note that with the source terms active, the edges of the wake rollup and form vortex bundles due to the strong mutual interaction between individual vortex filaments in these locations. This pairing of the tip vortices is the physically correct behavior as shown, e.g., in the experiments of Larin,[1] Müller,[27] and Heyson.[28]

Effect of Time-Step

One motivation for the present work was the need to have a computationally efficient, high-resolution wake algorithm for rotor/airframe interaction analysis and rotor acoustics. Explicit-type free-wake models exhibit numerical problems with small time-steps, and obviously cannot be used for such

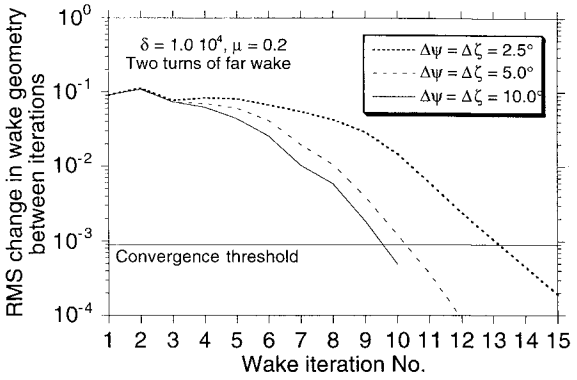

Fig. 5 Convergence characteristics of free-wake for high resolution temporal and spatial discretizations, $\mu = 0.2$, $C_T = 0.008$.

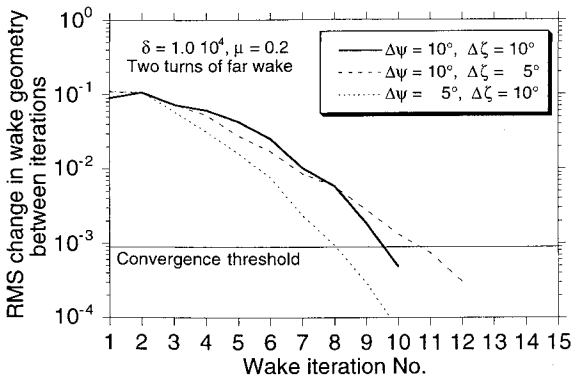

Fig. 6 Convergence characteristics of free-wake for unequal temporal and spatial discretizations, $\mu = 0.2$, $C_T = 0.008$.

problems. For acoustic work, a temporal step of the order of 1 deg of azimuth is necessary, and this is where the use of algorithms such as the present scheme prove beneficial.

The pseudoimplicit free-wake algorithm has been run for 10-, 5-, and 2½-deg azimuth steps, and the convergence characteristics are compared in Fig. 5. Note that with the higher resolution, the convergence with the present method takes place at a marginally slower rate, but is still fairly rapid. As discussed previously, the explicit method on the other hand, exhibits extremely poor convergence characteristics, often with many regular perturbations in the convergence histories.

It should also be realized that the computational effort required for higher resolution cases is significantly greater than for coarser discretizations. In fact, the CPU time increases approximately with the square of the number of grid points. The number of grid points depends on the length of the vortex filaments, the number of segments per filament, and the angular resolution in the azimuthal direction. If ζ_{max} represents the length of a vortex filament in radians, then the set of collocation points on the jth filament has

$$k_{max} = (\zeta_{max}/\Delta\zeta) + 1 \tag{25}$$

number of points, and so for an angular resolution $j_{max} = 2\pi/\Delta\psi$, the total number of collocation points in the rotor flowfield is $j_{max} \times k_{max}$. It is apparent that for the resolution necessary for acoustic predictions, tens of thousands of grid points are required.

Unequal Step Size

Obviously, the large number of velocity field evaluations associated with a high-resolution wake grid makes the computational time a major issue. However, note that the discretization of the computational domain in the ψ and ζ directions needs not be equal [see Eqs. (3), (4), (6), or (7)]. This feature can permit the use of a refined rotor azimuthal mesh without the added computational expense of a highly detailed wake grid. Alternatively, a detailed wake grid can be used with a less refined azimuth mesh. These features of the algorithm can be useful in several practical applications. For example, the former approach (small $\Delta\psi$ and larger $\Delta\zeta$) is potentially useful for some situations in rotor acoustic work where the induced velocity in the plane of the rotor is critical, but can be obtained with a coarser approximation to the wake geometry in the far field. On the other hand, the latter approach (larger $\Delta\psi$ and small $\Delta\zeta$) is useful in rotor/airframe interaction analyses where the accuracy in the wake geometry downstream, behind, and below the rotor is more important, and where the local fidelity of the blade loads can be sacrificed somewhat.

In addition to the foregoing, the ability to potentially invoke different steps in the ψ and ζ directions can be used to advantage in accelerating the overall wake convergence for a given fidelity, thereby minimizing computational requirements. This can be done by using larger ζ steps in the initial wake iterations, and progressively refining the wake as convergence begins. Since a substantial part of the overall CPU time is associated with repetitive evaluations of the Biot–Savart integral to find the induced velocity field, major gains in computational efficiency can be obtained by reducing the number of evaluations.

Figure 6 shows the convergence characteristics of the algorithm obtained for unequal temporal and spatial discretization, i.e., different values of $\Delta\psi$ and $\Delta\zeta$. It is important to note that the free-wake convergence characteristics remain essentially unchanged and are not compromised by such a scheme. The physical accuracy of the results is, however, compromised to some degree, since for unequal step sizes, information is no longer directly shifted along the characteristic lines that can be defined for the (hyperbolic) free-wake equation [Eq. (1)]. It can be rigorously shown that the scheme reduces to second-order accuracy for unequal step sizes, whereas discretization errors $\rightarrow 0$ when $\Delta\psi = \Delta\zeta$.

Comparison with Experiment

It has been previously mentioned that the selection of a tip vortex model (initial core size and viscous diffusion) influences both the rotor airloads and the wake rollup itself. The selection of a physically realistic vortex model is necessary to ensure that for young vortices that lie in the plane of the rotor and are responsible for blade vortex interactions (BVI) (with the associated high local airloads and impulsive noise generation), the tip vortex viscous core sizes and velocity profiles are physically realistic. Furthermore, since rotor performance and flowfield-induced velocity distributions are governed entirely by the position, strengths, and velocity profile of the tip vortices, the physical accuracy of the numerical scheme must be validated by comparison with experimentally obtained wake geometries.

It is known from experiments that older tip vortices diffuse somewhat, but with a time scale that is relatively long compared to the number of rotor revolutions. In some free-wake models, particularly those based on explicit schemes, the tip vortex "core radius" is often artificially large and is used to control or suppress numerical instabilities associated with close interactions between adjacent wake filaments, i.e., to force convergence. The physical accuracy of the predicted wake geometries is, however, the paramount issue at hand, and is not necessarily guaranteed by numerical convergence. To this effect, while it is still acceptable that in the "far" wake the tip vortex core radii may be larger than physical to alleviate some numerical problems inherent with some free-wake models, it is still imperative to ensure that a physical solution for the resulting wake be obtained.

Bearing these issues in mind, predicted wake geometry results using the present scheme have been compared with ex-

perimental measurements in order to establish the sensitivity of the numerical scheme to factors such as initial vortex core radii and diffusion rates (effective eddy viscosity). However, complete validation studies are difficult to conduct due to the lack of a consistent set of quantitative experimental data. Many experiments are incomplete, in that wake visualization data is available, but without simultaneous measurements of rotor thrust or trim state, therefore, severely limiting the scope of any study. While a considerable amount of flow visualization data are available for hovering flight conditions (e.g., Refs. 29–34), experimental data on the wake structure in forward flight are much rarer. References 8 and 35 provide some useful data, albeit in water tunnels, while Müller[27] has obtained a useful amount of data using smoke flow, but at subscale Mach numbers and for only one test condition.

Rotor wake visualization experiments have also been conducted under forward-flight conditions in Ref. 36 using the wide-field shadowgraph method. The rotor used was a four-bladed fully articulated rotor operating at close to full-scale tip Mach numbers. While an extensive validation study with all these data are beyond the scope of this article, some brief comparisons are discussed next.

The solution of the free-wake problem gives the aerodynamic velocity environment at the blade, and, therefore, the blade and rotor forces can be obtained by integration. However, a helicopter rotor is also a dynamic system with some form of articulation allowing flapping, lead-lag, and feathering (pitch) degrees of freedom. To make the computed results physically meaningful the rotor blades must be allowed to flap under the action of the aerodynamic forces and moments on each blade so that the rotor reaches an equilibrium position. This equilibrium also depends on the geometric and inertial characteristics of the rotor blades, but can be trimmed to obtain the required combination of rotor thrust and tip path plane angle of attack by the action of control inputs in the form of collective and cyclic pitch. The rotor trim routine was called at every iteration to ensure that the final solution for the wake geometry was fully compatible with the specified trim state. For the results computed in this article, the trim state was specified so that the rotor tip-path-plane (TPP) remained perpendicular to the rotor shaft.

Figure 7 shows measurements of the wake displacements at the longitudinal centerline of the upwind edge of the rotor in low-speed forward flight. For these conditions, there are significant changes to the wake geometry with small changes in rotor thrust or advance ratio, and so these cases provide a good general test of the capabilities of the free-wake model. Figure 7 clearly shows that the tip vortices generated at the upwind leading edge of the rotor disk move downstream, but are also convected over the top of the following blades. This result has been experimentally observed by Lehman,[7] Landgrebe et al.,[37] and others. At the longitudinal centerline, the largest vertical wake displacement above the TPP occurred at 90-deg of wake age, corresponding to the first blade passage below the vortex filament. For progressively greater wake ages, the wake is convected further downstream and downwards through the TPP. Despite the complexity of this process, the predictions are in good agreement with the measurements.

At the downwind edge of the disk, it can be seen from Fig. 8 that the vertical wake displacements were only very slightly affected by changes in advance ratio, i.e., the slopes (time rate of change of displacement or vertical velocity) were essentially constant. On the other hand, the effects of advance ratio on the streamwise displacements is more pronounced as might be expected, since in the absence of induced effects the streamwise convection is effectively proportional to advance ratio. Although it is difficult to see in Fig. 8, there is a small increment to the axial convection velocity of the rear wake at each subsequent blade passage with the introduction of a new tip vortex. Again, the agreement of the model with the

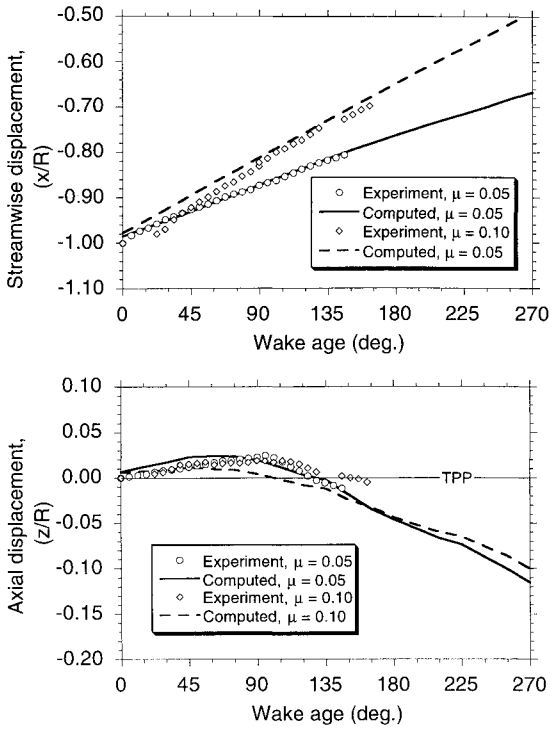

Fig. 7 Streamwise and vertical displacements vs wake age, upstream edge of rotor disk (shadowgraph data), $\alpha_s = -6$ deg, $C_T = 0.008$.

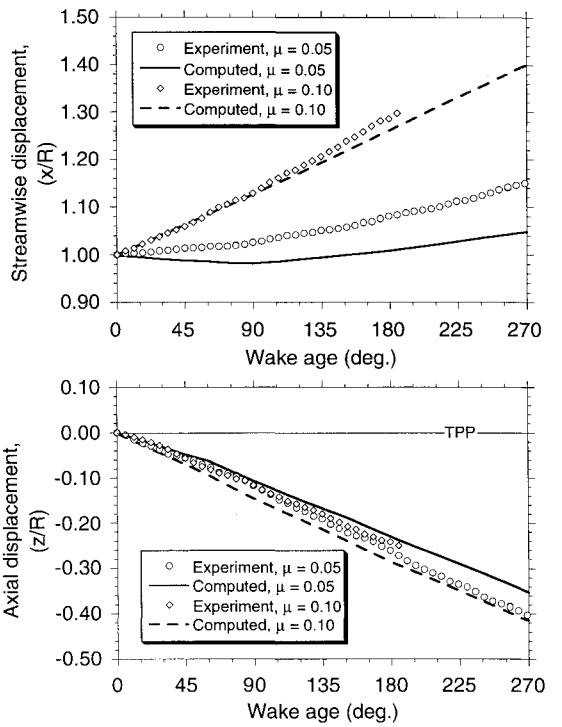

Fig. 8 Streamwise and vertical displacements vs wake age, downstream edge of rotor disk (shadowgraph data), $\alpha_s = -6$ deg, $C_T = 0.008$.

measurements is quite good. Comparisons of the predicted wake geometry with smoke flow visualization data obtained by Müller[27] are shown in Ref. 23.

The choice of δ is also an important factor in obtaining a physically realistic rotor wake solution. Figure 9 shows the effects of δ on the convergence trends of the numerical scheme, starting with an initial core radius of 25% chord. Physically, the tip vortex diffuses relatively slowly, but based on the

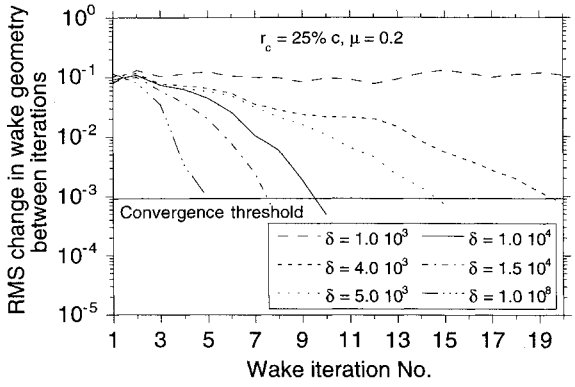

Fig. 9 Effect of the eddy viscosity coefficient on convergence trends, two turns of far wake, $\Delta\psi = 10$ deg $= \Delta\zeta$.

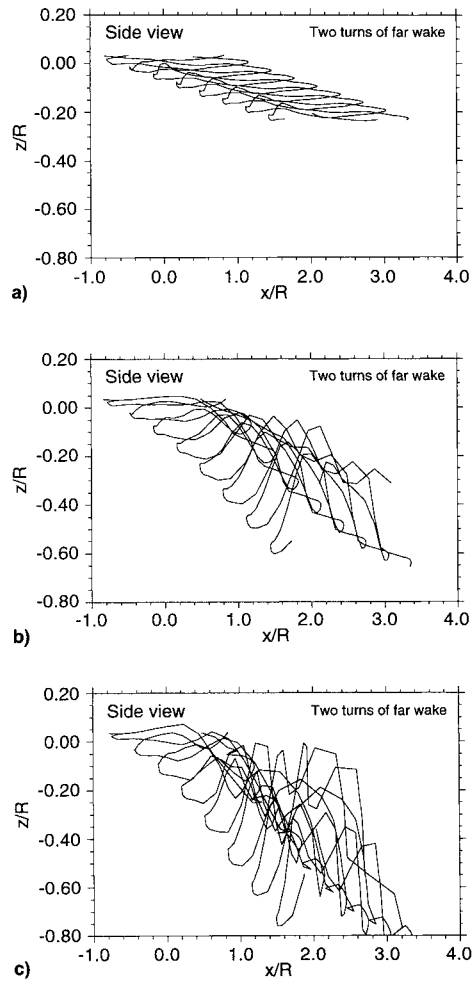

Fig. 10 Effect of eddy viscosity coefficient on predicted rotor wake geometries, $\mu = 0.2$, $\Delta\psi = 10$ deg $= \Delta\zeta$, δ = a) 10^8, b) 10^4, and c) 10^3.

results there might be a tendency to allow the core radius to grow at a greater rate. The problem is to ensure that this growth does not allow a nonphysical wake geometry to result. By using a very high decay rate ($\delta = 10^8$), the wake geometry can be forced to relax to a converged solution within five iterations. However, the wake geometry corresponding to this decay rate does not capture the distortion and rollup of the wake as observed experimentally (e.g., Ref. 27).

It is also interesting to note that the effect of increasing δ is equivalent to reducing the mutual influence between the wake vortices, (i.e., reducing the influence of the source terms) and as $\delta \to \infty$ the predicted wake geometry approaches the undistorted wake given by Eq. (10). The use of a very small value of δ, on the other hand, results in very strong mutual interference effects between the tip vortices, producing a highly distorted wake structure. In this case, comparison with experimental data suggests an overprediction of the wake distortion. Figure 10 shows the tip vortices trailed from a rotor blade at $\psi_b = 0$ deg for a four-bladed rotor, for three values of δ, and serves to illustrate the sensitivity of the converged wake geometry to the decay rate. Clearly, the choice of the eddy viscosity coefficient is critical to the prediction of the wake geometry.

Summary and Conclusions

A new free-wake model has been developed to predict the tip vortex structure and flowfield velocities in a rotor wake. The model is based on a pseudoimplicit formulation with five-point central differencing in space, and is implemented as a two-step predictor–corrector relaxation scheme. A numerical analysis has been conducted to examine the convergence characteristics of the method and its suitability for general application to aerodynamic problems involving rotors. The robustness of the scheme has been demonstrated for a wide range of flight conditions. A brief comparison with experimental measurements of rotor wake geometries in forward flight showed good agreement, although further validation studies must still be performed.

Since the present method is implemented as a predictor–corrector scheme, it requires about twice the computational effort per iteration compared to single-step explicit methods. However, it has been shown that this new scheme is much more robust and much less susceptible to numerical instabilities than more typical explicit-type free-wake methods. Furthermore, the method has demonstrated very fast convergence for relatively small spatial/temporal discretizations of the wake, a feature that is essential for rotor acoustic predictions. The generalized discretization scheme used here also permits the use of unequal time and space step increments that may be useful in several other practical applications of the wake model.

Appendix A: Shift Operator

The shift operator E can be viewed as a notational form of representing the change of the index of a variable. For example,

$$E_\psi^{-1} \boldsymbol{r}_{j,k}^n \equiv \boldsymbol{r}_{j-1,k}^n$$

$$E_\zeta^{-1} \boldsymbol{r}_{j,k}^n \equiv \boldsymbol{r}_{j,k-1}^n$$

$$E_\psi^{-1} E_\zeta^{-1} \boldsymbol{r}_{j,k}^n \equiv \boldsymbol{r}_{j-1,k-1}^n$$

Using this notational form, it is convenient to rewrite the standard delta form as a matrix equation as in Eq. (21).

Appendix B: Exact Solution in One Iteration

Recall that $\Delta \boldsymbol{r}^n = \boldsymbol{r}^{n+1} - \boldsymbol{r}^n$. Substituting this definition into Eq. (21), we have for the pseudoimplicit method

$$[I]\{\boldsymbol{r}^{n+1} - \boldsymbol{r}^n\} = -[I]\{\boldsymbol{r}^n\} - [P]^{-1}\{\boldsymbol{bc} + S\} \quad \text{(B1)}$$

which reduces to

$$\{\boldsymbol{r}^{n+1}\} = -[P]^{-1}\{\boldsymbol{bc} + S\} \quad \text{(B2)}$$

similarly,

$$\{\boldsymbol{r}^{n+2}\} = -[P]^{-1}\{\boldsymbol{bc} + S\} \quad \text{(B3)}$$

Hence, $\{\boldsymbol{r}^{n+1}\}$ is not an explicit function of $\{\boldsymbol{r}^n\}$, but is dependent only upon the P operator, the boundary conditions $\boldsymbol{bc}$,

and the constant source terms S. For the previous method, P is defined by Eq. (20) for the pseudoimplicit method. Note that the previous one-iteration solution is a consequence of the iteration scheme used, as reflected by the P operator.

Acknowledgments

This work was partly supported by the U.S. Army Research Office under Contract DAAH-04-93-G-001. The authors would like to thank James Baeder for helpful discussions.

References

[1]Larin, A. V., "Vortex Wake Behind a Helicopter," *Aviatsiya i kosmonavtika*, No. 3, 1973, pp. 32–33; also National Technical Infomation Service, ADA005479 (translation), 1974.

[2]Larin, A. V., "Vortex Formation in Oblique Flow Around a Helicopter Rotor," *Uchenyye Zapiski TSAGI*, Vol. 1, No. 3, 1970, pp. 115–122; also National Technical Information Service, AD781245 (translation), 1974.

[3]Landgrebe, A. J., "An Analytical and Experimental Investigation of Helicopter Rotor Performance and Wake Geometry Characteristics," U.S. Army Air Mobility Research and Development Lab., TR 71-24, June 1971.

[4]Kocurek, J. D., and Berkowitz, L. F., "Velocity Coupling—A New Concept for Hover and Axial Flow Wake Analysis and Design," AGARD CP 334, May 1982.

[5]Egolf, T. A., and Landgrebe, A. J., "Helicopter Rotor Wake Geometry and Its Influence in Forward Flight, Vol. I–Generalized Wake Geometry and Wake Effect on Rotor Airloads and Performance," NASA CR-3726, Oct. 1983.

[6]Beddoes, T. S., "A Wake Model for High Resolution Airloads," *Proceedings of the 2nd International Conference on Basic Rotorcraft Research* (Triangle Park, NC), American Helicopter Society, 1985.

[7]Lehman, A. F., "Model Studies of Helicopter Rotor Flow Patterns," U.S. Army Aviation Material Lab., TR 68-17, April 1968.

[8]Landgrebe, A. J., and Bellinger, E. D., "An Investigation of the Quantitative Applicability of Model Helicopter Rotor Wake Patterns Obtained from a Water Tunnel," United Aircraft Research Lab., K910917-23, Dec. 1971.

[9]Clark, D. R., and Leiper, A. C., "The Free Wake Analysis—A Method for the Prediction of Helicopter Rotor Hovering Performance," *Journal of the American Helicopter Society*, Vol. 15, No. 1, 1970, pp. 3–11.

[10]Landgrebe, A. J., "An Analytical Method for Predicting Rotor Wake Geometry," *Journal of the American Helicopter Society*, Vol. 14, No. 4, 1969, pp. 20–32.

[11]Sadler, S. G., "Development and Application of a Method for Predicting Rotor Free Wake Positions and Resulting Rotor Blade Air Loads," *Model and Results*, Vol. 1, NASA CR 1911, Dec. 1971.

[12]Scully, M. P., "Computation of Helicopter Rotor Wake Geometry and Its Influence on Rotor Harmonic Airloads," Massachusetts Inst. of Technology Aeroelastic and Structures Research Lab., ASRL TR 178-1, Cambridge, MA, March 1971.

[13]Bliss, D. B., Wachspress, D. A., and Quackenbush, T. R., "A New Approach to the Free Wake Problem for Hovering Rotors," *Proceedings of the 41st Annual Forum of the American Helicopter Society* (Fort Worth, TX), American Helicopter Society, 1985, pp. 463–477.

[14]Egolf, T. A., "Helicopter Free Wake Prediction of Complex Wake Structures Under Blade-Vortex Interaction Operating Conditions," *Proceedings of the 44th Annual Forum of the American Helicopter Society* (Washington, DC), American Helicopter Society, 1988.

[15]Quackenbush, T. R., Bliss, D. B., and Wachspress, D. A., "Computational Analysis of Hover Performance Using a New Free Wake Method," *Proceedings of the 2nd International Conference on Rotorcraft Basic Research* (College Park, MD), American Helicopter Society, 1988.

[16]Miller, W. O., and Bliss, D. B., "Direct Periodic Solutions of Rotor Free Wake Calculations by Inversion of a Linear Periodic System," *Proceedings of the 46th Annual Forum of the American Helicopter Society* (Washington, DC), American Helicopter Society, 1990, pp. 757–769.

[17]Widnall, S. E., "The Stability of a Helical Vortex Filament," *Journal of Fluid Mechanics*, Vol. 54, No. 4, 1972, pp. 641–663.

[18]Johnson, W., "A Comprehensive Analytical Model of Rotorcraft Aerodynamics and Dynamics," NASA TM-81182, June 1980.

[19]Bir, G., and Chopra, I., "University of Maryland Advanced Rotor Code (UMARC) Theory Manual," Univ. of Maryland, Center for Rotorcraft Education and Research, UM-AERO 92-02, College Park, MD, Nov. 1992.

[20]Stoer, J., and Bulirsch, R., *Introduction to Numerical Analysis*, Springer–Verlag, New York, 1983.

[21]Crouse, G. L., and Leishman, J. G., "A New Method for Improved Free-Wake Convergence in Hover and Low Speed Forward Flight," AIAA 31st Aerospace Sciences Meeting and Exhibit, Reno, NV, Jan. 1993.

[22]Rossow, V. J., "On the Inviscid Rolled-Up Structure of Lift Generated Vortices," *Journal of Aircraft*, Vol. 10, No. 11, 1973, pp. 647–650.

[23]Bagai, A., and Leishman, J. G., "Rotor Free-Wake Modeling Using a Pseudo-Implicit Technique—Including Comparisons with Experimental Data," *Journal of the American Helicopter Society*, Vol. 40, No. 3, 1995, pp. 29–41.

[24]Lamb, H., *Hydrodynamics*, 6th ed., Cambridge Univ. Press, Cambridge, MA, 1932, pp. 592, 593, 668, 669.

[25]Ogawa, A., *Vortex Flow*, CRC Press, Boca Raton, FL, 1993.

[26]Squire, H. B., "The Growth of a Vortex in Turbulent Flow," *Aeronautical Quarterly*, Vol. 16, Aug. 1965, pp. 302–306.

[27]Müller, R. H. G., "Winglets on Rotor Blades in Forward Flight—A Theoretical and Experimental Investigation," *Vertica*, Vol. 14, No. 1, 1990, pp. 31–46.

[28]Heyson, H. H., and Katzoff, S., "Induced Velocities Near a Lifting Rotor with Non-Uniform Disk Loading," NACA TR 1319, 1957.

[29]Landgrebe, A. J., "The Wake Geometry of a Hovering Rotor and Its Influence on Rotor Performance," *Journal of the American Helicopter Society*, Vol. 17, No. 4, 1972, pp. 2–15.

[30]Sullivan, J. P., "An Experimental Investigation of Vortex Rings and Helicopter Rotor Wakes Using a Laser Doppler Velocimeter," Massachusetts Inst. of Technology, MIT DSR 80038, Cambridge, MA, June 1973.

[31]Tangler, J. L., Wohlfeld, R. M., and Miley, S. J., "An Experimental Investigation of Vortex Stability, Tip Shapes, Compressibility, and Noise for Hovering Model Rotors," NASA CR-2305, Sept. 1973.

[32]Tung, C., Pucci, S. L., Caradonna, F. X., and Morse, H. A., "The Structure of Trailing Vortices Generated by Model Helicopter Rotor Blades," *Vertica*, Vol. 7, No. 1, 1983, pp. 33–43.

[33]Bagai, A., and Leishman, J. G., "A Study of Rotor Wake Developments and Wake/Body Interactions in Hover," *Journal of the American Helicopter Society*, Vol. 37, No. 4, 1992, pp. 48–57.

[34]Landgrebe, A., "An Analytical and Experimental Investigation of Helicopter Rotor Performance and Wake Geometry Characteristics," U.S. Army Air Mobility Research and Development Lab., TR 71-24, June 1971.

[35]Erikson, G. H., "Flow Visualization Study of Helicopter Tip Vortices Using a Four-Bladed Rotor System," Massachusetts Inst. of Technology, Cambridge, MA, March 1970.

[36]Leishman, J. G., and Bagai, A., "Fundamental Studies of Rotor Wakes in Low Speed Forward Flight Using Wide-Field Shadowgraphy," *Proceedings of the AIAA 9th Applied Aerodynamics Conference* (Baltimore, MD), AIAA, Washington, DC, 1991.

[37]Landgrebe, A. J., Taylor, R. B., Egolf, T. A., and Bennett, J. C., "Helicopter Airflow and Wake Characteristics for Low Speed and Hovering Flight from Rocket Interference Investigations," *Journal of the American Helicopter Society*, Vol. 27, No. 4, 1982, pp. 74–83.